Available online at www.sciencedirect.com

SciVerse ScienceDirect

Ceramics International 38 (2012) 1617–1625

CERAMICS INTERNATIONAL

www.elsevier.com/locate/ceramint

Microstructure and mechanical behavior of alumina–zirconia–mullite refractory materials

G.I. Vázquez Carbajal *, J.L. Rodríguez Galicia, J.C. Rendón Ángeles, J. López Cuevas, C.A. Gutiérrez Chavarría

Centro de Investigación y de Estudios Avanzados del Instituto Politécnico Nacional-Unidad Saltillo, Carretera Saltillo-Monterrey Km 13.5, C.P. 25900, Ramos Arizpe, Coahuila, Mexico

Received 14 June 2011; received in revised form 20 September 2011; accepted 27 September 2011

Available online 4 October 2011

Abstract

The synthesis of Al_2O_3–ZrO_2–SiO_2 (AZS) refractory materials for use in furnace chambers for glass melting has been studied in this work. Several mixtures with different alumina–zirconia–silica ratios, corresponding to compositions selected within the ternary phase diagram Al_2O_3–ZrO_2–SiO_2, were processed by attrition milling followed by pressing and reactive sintering at different temperatures (1450, 1550 and 1650 °C). The density of the sintered samples varied significantly with respect to that of the green materials, with increases of up to 90% in this property after sintering at 1650 °C. The X-ray diffraction patterns revealed the formation of the predicted phases (ZrO_2, $Al_6Si_2O_{13}$ and Al_2O_3) according to the ternary phase diagram for all compositions studied, with varying amounts of each formed phase. SEM characterization showed that the sintering temperature employed made a significant difference regarding the final microstructure of the sintered materials. For the studied compositions, the maximum resistance to fracture (MRF) was 185 MPa, with the highest values of fracture toughness obtained at 1650 °C.

Keywords: AZS refractories; ZrO_2; Microstructure; Mechanical properties

1. Introduction

Glass melting furnaces are the most expensive pieces of equipment within the glass industry. Furnace costs include installation, operation and maintenance expenses. To make glass products competitive compared to plastic, aluminum, and cardboard packaging; their production cost must be reduced [1]. The refractory industry is currently designing and developing new materials that meet the technical needs of the furnaces in the glass industry at lower costs.

The research work carried out so far has shown that the strongest attack by corrosion suffered by the refractories of the glass melting furnaces occurs in the area where the fully melted glass is in contact with the refractory. Therefore, it is essential to provide the greatest resistance to corrosion of the refractory liners used in that area. AZS type materials have been widely used by the glass industry [2] since they allow achieving longer warranty periods and improve the quality of the produced glass.

AZS type materials consist mainly of corundum, mullite and zirconia. Alumina has high hardness and good corrosion resistance, but also has a relatively low fracture toughness compared to zirconia; which exhibits high strength and good fracture toughness, but has low hardness [3]. Refractory materials with ZrO_2 contents ranging from 31 to 42 wt.% are manufactured by melting and casting, and are characterized by high corrosion resistance toward several types of aggressive environments [4]. However, the presence of ZrO_2 in AZS refractories causes a significant change in volume of about 3–5% above 1000 °C due to tetragonal to monoclinic phase transformation in ZrO_2, which corresponds to a martensitic transformation. During cooling of the material, the martensitic transformation causes the formation of microcracks and porosity, with a decrease in mechanical strength, associated with a reduction in its Young's modulus [5,6]. The volume change can be dissipated by the presence of a glassy phase, which constitutes approximately 30% of the volume of the AZS type materials [7–9]. When suitable crystalline/glass phase

---

* Corresponding author. Tel.: +52 844 438 9600x9683; fax: +52 844 438 9610.

E-mail address: givazquez@hotmail.com (G.I.V. Carbajal).

0272-8842/$36.00 © 2011 Elsevier Ltd and Techna Group S.r.l. All rights reserved.
doi:10.1016/j.ceramint.2011.09.051

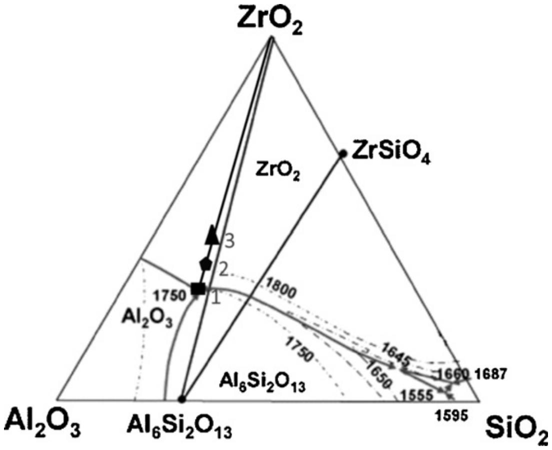

Fig. 1. Ternary system Al_2O_3–ZrO_2–SiO_2 [10].

Table 1
Alumina–zirconia–silica ratios for compositions selected in the ternary system Al_2O_3–ZrO_2–SiO_2.

Composition	Al_2O_3 (wt.%)	SiO_2 (wt.%)	ZrO_2 (wt.%)
C1	51.79	15.83	32.37
C2	45.3	14.4	40.3
C3	38.13	11.5	50.36

relationships are obtained, AZS materials will have an optimal performance during use. Different phase relationships in the microstructure can significantly impact the lifetime of these materials. The main aim of this work is to develop suitable AZS type refractory materials constituted by the appropriate crystalline phases so as to allow their optimal performance in furnaces used for glass manufacturing.

2. Experimental procedure

An optimal relationship for the distribution of fine particles in the selected alumina–zirconia–silica compositions was established by studying the ternary system Al_2O_3–ZrO_2–SiO_2 shown in Fig. 1 [10]. The selected compositions were prepared by using suitable mixtures of the employed raw materials, and high-energy attrition milling, followed by axial pressing and reactive sintering at different temperatures (1450, 1550 and 1650 °C). The sintering temperatures were established according to the relevant invariant points in the ternary system Al_2O_3–ZrO_2–SiO_2. The employed alumina–zirconia–silica ratios, given in Table 1, were determined for the compositions indicated in the ternary phase diagram of Fig. 1.

The raw materials used in this study were Sasol α-alumina (99.995% of purity), non-stabilized zirconia superfine grade from Inframat Advanced Materials, and Mineral Kaolin from Koprimo SA de CV. The latter mineral was used as a source of silica, mainly due to the problems encountered in a previous work [11], where pure silica was used as a raw material. The average particle size ranged from 1 to 9 μm for all employed raw materials.

In order to carry out an appropriate mass balance to introduce the required percentage of silica in each one of the studied compositions, the chemical composition of kaolin was analyzed by Inductively Coupled Plasma Emission spectroscopy (Intrepid II XSP Iris apparatus) as well as by Atomic Absorption Spectroscopy (Thermo Electron Corporation Solar S4 apparatus); the results are shown in Table 2. The batch compositions shown in Table 3 were calculated by taking into account the water of hydration loss for kaolin.

The mixture powders were subjected to grinding in an attrition mill, which was followed by axial pressing at 55 MPa using a CARVER INC 4350 press with a capacity of 11 tons in order to obtain rectangular preforms with dimensions of 7 cm length, 3 cm width and 4 cm depth prior to sintering at different temperatures (1450, 1550 and 1650 °C). The samples were sintered in a Thermoline 46200 high temperature furnace; using a heating and cooling rate of 2 °C/min and a dwell time of 5 h at the maximum temperature. Crystalline phases in the sintered samples were analyzed by X-ray diffraction using a Philips PW3040 X'pert diffractometer equipped with a vertical goniometer; CuKα radiation, with $\lambda = 1.5418$ Å, a working voltage of 40 kV, a current of 30 mA and a scanning speed of 0.02° 2θ/seg, in the 10–80° 2θ range.

The densities of the samples were measured by immersion in mercury using the Archimedes' principle. The elastic modulus (E) was measured at room temperature using ultrasonic testing, employing the pulse-echo technique based on Eq. (1); where V_L = longitudinal velocity of the ultrasonic wave and ρ = density of the material. The longitudinal velocity of ultrasonic wave for each one of the Al_2O_3–SiO_2–ZrO_2 compositions studied was obtained. For this test, an ultrasonic inspection system (Perametrics Poch 4) was used; with different sized fixtures [all of them greater than 5 mm (0.2 in.) of thickness according to ASTM E494-95 [12] and ASTM E 797-95 [13]]. The measured values were compared with those calculated from stress–strain curves obtained from three-point bending tests.

$$E = \frac{(V_L)^2(\rho)}{1.499} \tag{1}$$

The modulus of rupture (MOR) was determined by three-point bend testing using a Material Test System MTS 810 hydraulic equipment with a cell capacity of 10 Ton, applying a cross-head speed of 0.5 mm/min, according to the ASTM C1161-94 standard [14]. After sintering the preforms were sectioned according to ASTM, the dimensions of the flexure bars were 4 mm width × 3 mm depth × 45 mm length. Edges of the bars

Table 2
Chemical analysis of kaolin (wt.%).

SiO_2	Al_2O_3	Fe_2O_3	TiO	P_2O_5	CaO	MgO	K_2O	Na_2O	Loss on ignition
45.73	37.36	0.79	0.37	0.236	0.18	0.098	0.33	0.059	13.91

Table 3
Alumina–zirconia–silica ratios for compositions selected in the ternary system Al_2O_3–ZrO_2–SiO_2.

Composition	Al_2O_3 (wt.%)	$Al_2Si_2O_5\ (OH)_4$ (wt.%)	ZrO_2 (wt.%)
C1	33.01	34.61	32.37
C2	28.21	31.49	40.3
C3	24.49	25.14	50.36

were slightly chamfered at a 45° angle to reduce tensile stresses, with a minimum of five tests made at a given temperature.

Vickers microhardness was measured by application of a load using a diamond indenter of pyramidal geometry [15] according to ASTM E92-82 [15]. Indentations were made on polished specimens with a load of 8, ten tests measured for each composition. The hardness was calculated from the diagonal length of the indentation optically determined for each indentation, using the following Eq. (2) where HV is Vickers hardness, P is applied load (kg) and d is mean of the diagonal length of indentations (mm).

$$HV = \frac{1.8544P}{d^2} \tag{2}$$

Fracture toughness (K_{Ic}) values were determined by the indentation technique using Eq. (3), where HV = Vickers microhardness, E = Young's modulus, c = length of the indentation mark and a = total length of the cracks formed at the tips of the indentation marks.

$$K_{\mathrm{Ic}} = 0.048 \times \left(\frac{c}{a}\right)^{-1.32} \times \left(\frac{E}{HV}\right)^{0.4} \times HV \times \sqrt{a} \tag{3}$$

The different phases formed during the heat treatments were analyzed by Scanning Electron Microscopy (SEM), using a Phillips XL30 ESEM microscope, with tungsten filament and equipped with a Genesis EDAX microanalyzer. The operating conditions employed were: accelerating voltage of 25 kV, working distance of 8 mm and analysis time of 30 s. All the fracture surfaces of the flexure bars were examined for failure origins by optical microscopy and SEM.

3. Results and discussion

3.1. X-ray diffraction (XRD)

XRD patterns of samples of composition C1 sintered at 1450 (T1), 1550 (T2) and 1650 °C (T3) are shown in Fig. 2. These patterns show mainly the presence of four crystalline phases: monoclinic ZrO_2, tetragonal ZrO_2, $Al_6Si_2O_{13}$ and $ZrSiO_4$. With increasing temperature, the intensity of the zirconia peaks increases, while that of mullite peaks decreases. This change is associated with a corresponding increase in the amount of the former phase and a decrease in that of the latter one.

The characteristic peaks of zircon (20° 2θ) has a very low intensity at 1450 °C. These peaks disappear when temperature is increased above 1450 °C due to the reaction occurring between SiO_2 of kaolin and alumina, which leads to the formation of zirconia and mullite. Thus, at temperatures higher than 1450 °C, the amount of these two phases increases.

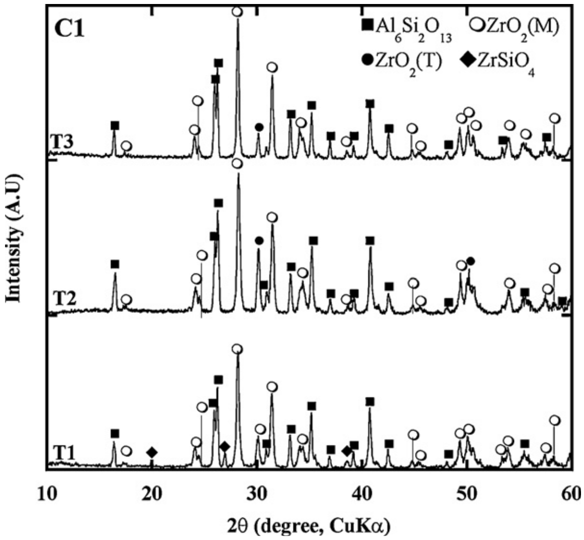

Fig. 2. X-ray diffraction patterns of composition C1 sintered at T1 = 1450, T2 = 1550 and T3 = 1650 °C (○ monoclinic ZrO_2, ● tetragonal ZrO_2, ◆ $ZrSiO_4$, and ■ $Al_6Si_2O_{13}$).

The X-ray diffraction patterns for compositions C2 and C3 are shown in Fig. 3. Both patterns are very similar. At 1450 °C we can observe an increase in the intensity of the peaks corresponding to mullite and zirconia phases, as well as the presence of a small amount of zircon. The latter phase is thought to have been formed mainly due to the reassociation [16] of zirconia with silica for kaolin at temperatures between 1300 °C and 1450 °C. The zirconia and silica interactions are associated with the occurrence of surface nucleation as well as with an increased growth of zircon crystals. At higher temperatures the zircon crystals disappear due to their dissociation back into zirconia and silica [16]. Even though composition C1 corresponds to the eutectic point of the ternary system, we did not observe the presence in its microstructure of phases with the eutectic morphology characteristic of electrofused materials.

In composition C3, the proportion of the formed phases was lower compared to that observed for composition C2, which was due to a higher content of alumina and silica than in the latter one. By increasing temperature to 1550 °C and 1650 °C, we see that mullite and zirconia phases are present in larger proportions in both compositions C2 and C3.

3.2. Microstructural characterization

SEM micrographs of samples treated at different temperatures are shown in Figs. 4–6. The differences in the microstructures are due to the percentage of zirconia, alumina and silica added to the mixtures in the compositions, and the phases formed during heat treatment. In the micrographs corresponding to composition C1 (Fig. 4) we can observe the microstructural changes that took place during the heat treatments. A homogeneous microstructure consisting of bright white ZrO_2 particles with a size ranging from 2 to 4 μm is

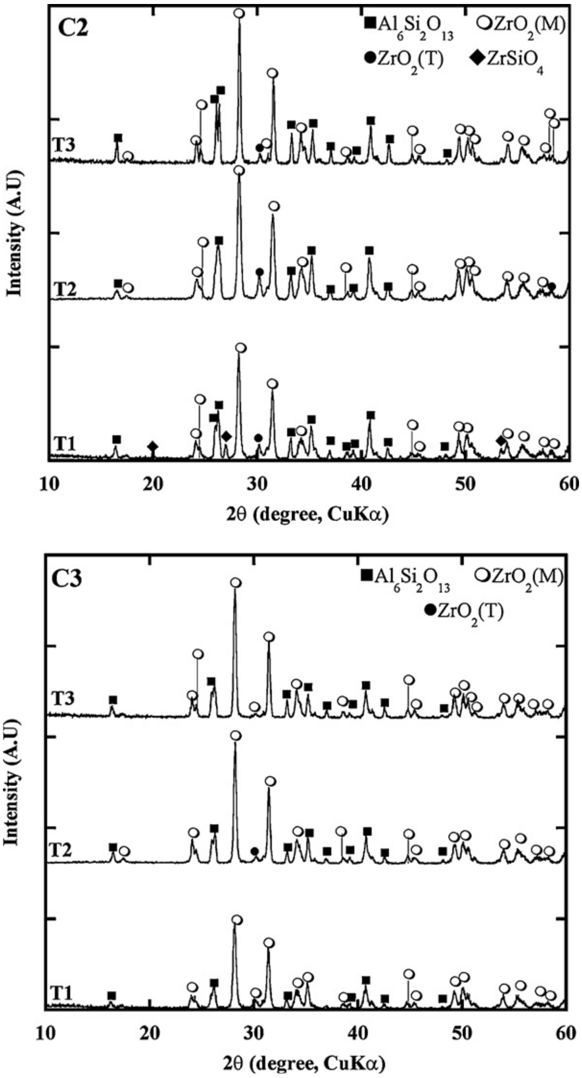

Fig. 3. X-ray diffraction patterns of compositions C2 and C3 sintered at T1 = 1450, T2 = 1550 and T3 = 1650 °C (○ monoclinic ZrO_2, ● tetragonal ZrO_2, and ■$Al_6Si_2O_{13}$).

noted. In these micrographs, mullite is the matrix phase in the microstructure.

An increase in temperature from 1450 to 1550 °C and from 1550 to 1650 °C caused an increase in the amount of zirconia particles with sizes from ~500 to 900 nm for the first temperature and ~2 μm for the second one. The considerable increase observed in the ZrO_2 particle size when temperature is raised from 1550 to 1650 °C can be attributed to the generation of a transitory liquid phase that promotes grain growth in the liquid state.

The photomicrographs of Figs. 5 and 6, corresponding to compositions C2 and C3. Both compositions are located in the primary crystallization field of alumina in the ternary system Al_2O_3–ZrO_2–SiO_2, and show the presence of three crystalline phases predicted by the corresponding compatibility triangle: Al_2O_3, ZrO_2 and $Al_6Si_2O_{13}$. We also notice that there is no significant difference in the formed phases, except for a slightly larger ZrO_2 particle size for the case of composition C2 sintered at 1650 °C. For both compositions C2 and C3 and all three sintering temperatures employed, mullite constitutes the matrix phase and zirconia is homogeneously distributed throughout the microstructure, with nanometric particles of the latter phase present in some cases. It can also be seen that alumina is embedded in the matrix phase in the form of small and irregularly shaped dark particles, which are homogeneously distributed. When temperature is increased to 1550 and 1650 °C alumina is not present as part of the matrix, mainly because its reaction with the silica from kaolin to produce mullite present in the microstructure.

During the microstructural analysis of each of the samples, a study was conducted using the X-ray dispersive energy technique, in order to carry out a semiquantitative study on the composition of the phases in each of the studied compositions. This study was conducted by obtaining the spectrum of composition using a 1 μm^2 micro-area. The micrographs obtained at 3000× are shown in Fig. 7, where you can see clearly the formed phases. Additionally, the X-ray energy dispersive spectra are shown, where you can see the semiquantitative proportion of elements present, which are the result of the specific analysis for each of the phases. The micrographs shown in Fig. 7 are sintered at 1450 °C. One can see the matrix is predominately mullite with alumina present due to the composition of the mixture.

3.3. Consolidation

Axially pressed preforms of all compositions studied were sintered at 1450–1650 °C. The apparent densities of both the green and the sintered samples are shown in Fig. 8. The percentage of porosity for the green samples is in the range of 48–52% relative to the theoretical density. The theoretical densities of the composites were estimated by the rule of mixtures, using 4.12 and 4.58 g/cm^3 for the theoretical densities of compositions. For all materials, after sintering at temperatures up to 1650 °C, density increases up to 90% over the value corresponding to the green samples were observed. As it is well known, this effect is mainly due to the physicochemical changes occurring during the initial stage of the sintering process, which involves a rearrangement of the particles as well as the formation of necks at their contact points by diffusion, vapor transport, plastic flow and/or viscous flow. This neck growth is accompanied by densification of the material [17]. Besides causing an increase in density as well as a decrease in porosity, an increase in the sintering temperature also enhances the reactivity between the particles. This is accentuated by the high energy milling given to the raw materials prior to their heat treatment, which leads to a better reaction in the latter stage due to a higher specific surface area and more intimate mixture of the particles in the milled material [7–9]. This results in a homogeneous distribution of the particles in the final microstructure of the sintered materials. One disadvantage of composition C1 is that it has low density; which is attributed mainly to the high proportion of kaolin added to this composition, making it more prone to the generation of cracks as a consequence of the volumetric changes associated with the transformation of kaolin into metakaolin [18].

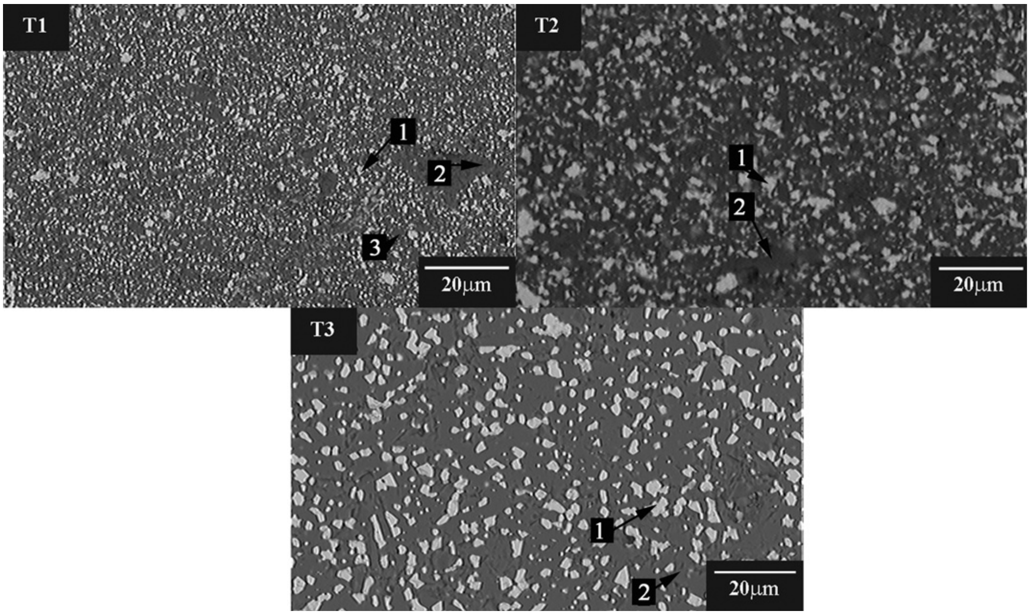

Fig. 4. Microstructures of composition C1 sintered at T1 = 1450 °C, T2 = 1550 °C and T3 = 1650 °C; (1) ZrO_2, (2) $Al_6Si_2O_{13}$ and (3) Al_2O_3.

3.4. Young's modulus

The Young's modulus was calculated using the pulse-echo ultrasound technique; with the results shown in Fig. 9. At 1650 °C the measured values were highest because the samples achieved the best densification. The values obtained by ultrasound measurements were compared with those calculated from the slope of the stress–strain curves obtained by three-point bending testing. In general, it can be seen that there is no significant variation between the values of the Young's modulus obtained using both methods, the slightly difference is mainly because in the experiments made for this investigation was observed that the mechanical tests are more sensible to the distribution of defects in the samples.

3.5. Modulus of rupture (MOR)

All compositions studied in this work were prepared by using zirconia as a raw material. For these materials, the maximum resistance to fracture (MRF) obtained was 185 MPa at 1650 °C, as shown in Fig. 10. This value is lower than that (293 MPa) reported in another experiments for similar refractories obtained by using zircon as raw material. In the latter case, the homogeneous distribution of ZrO_2 throughout

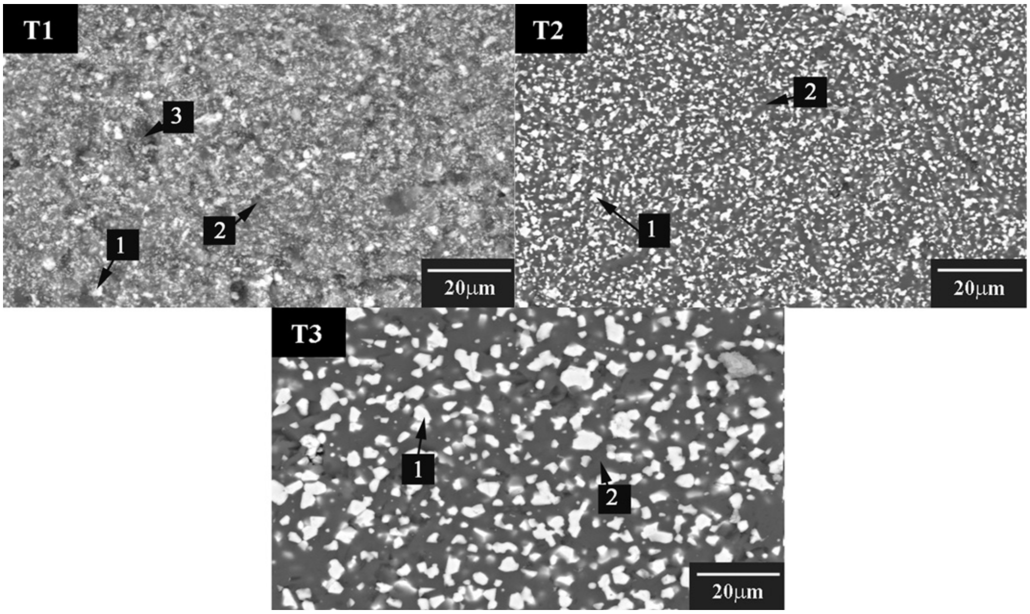

Fig. 5. Microstructures of composition C2 sintered at T1 = 1450 °C, T2 = 1550 °C and T3 = 1650 °C; (1) ZrO_2, (2) $Al_6Si_2O_{13}$ and (3) Al_2O_3.

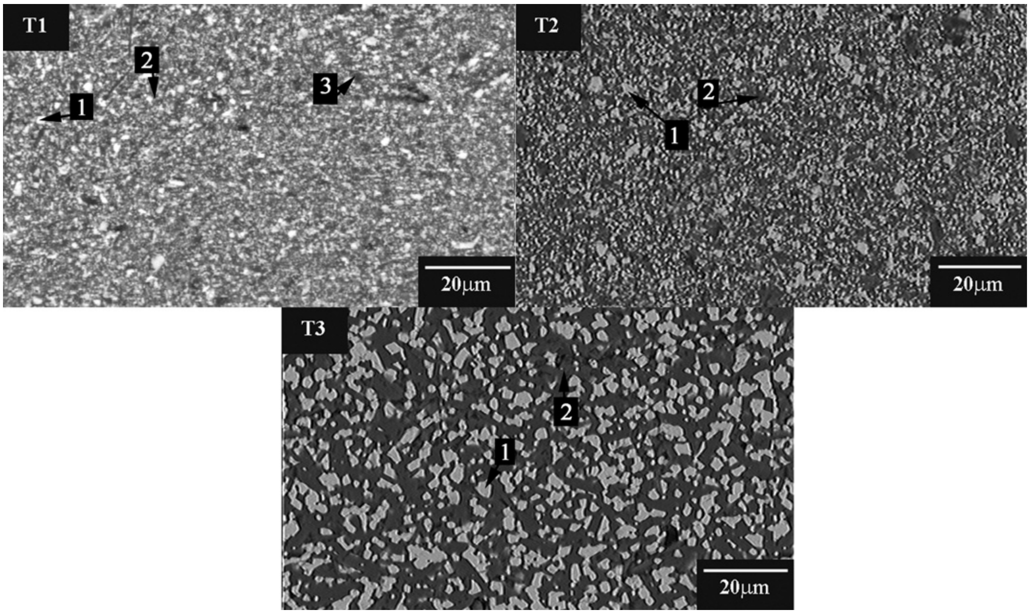

Fig. 6. Microstructures of composition C3 sintered at T1 = 1450 °C, T2 = 1550 °C and T3 = 1650 °C; (1) ZrO_2, (2) $Al_6Si_2O_{13}$ and (3) Al_2O_3.

the matrix might be responsible for the observed increase in the mechanical properties. It is well known that ceramic materials can show experimental values for their mechanical properties which are lower than the theoretical ones due to the presence of defects caused by porosity, impurities, agglomerates, etc.; which have different sizes, shapes and orientation; and which can act as stress concentration centers [19]. Therefore, two specimens of the same material, identical in principle, may not have an equal distribution of defects, so that their tensile strength and toughness will be different [19]. This could explain

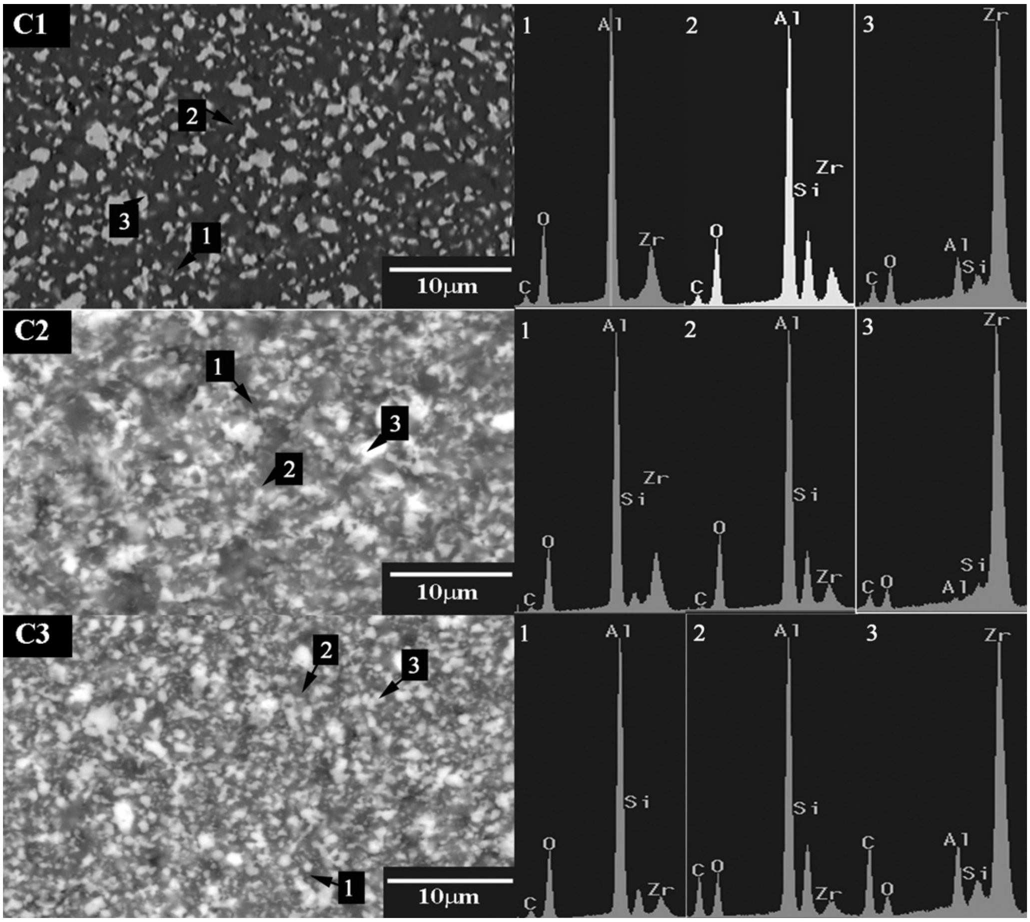

Fig. 7. X-ray energy dispersive spectra of compositions C1, C2 and C3 sintered at 1450 °C, (1) Al_2O_3, (2) $Al_6Si_2O_{13}$ and (3) ZrO_2.

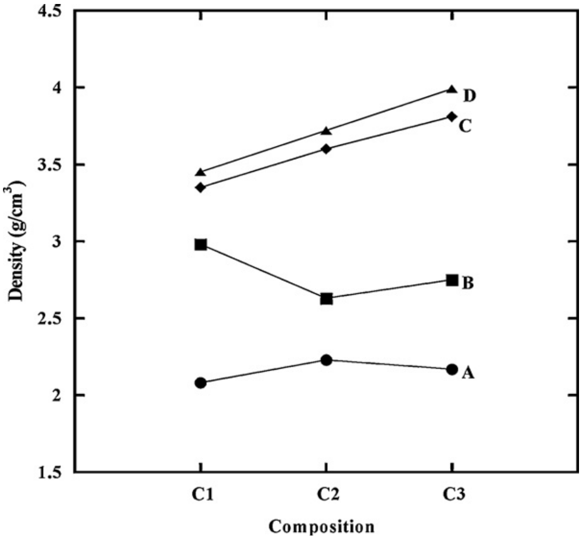

Fig. 8. Density of A = green samples (●) and of samples sintered at B = 1450 °C (■), C = 1550 °C (◆) or D = 1650 °C (▲).

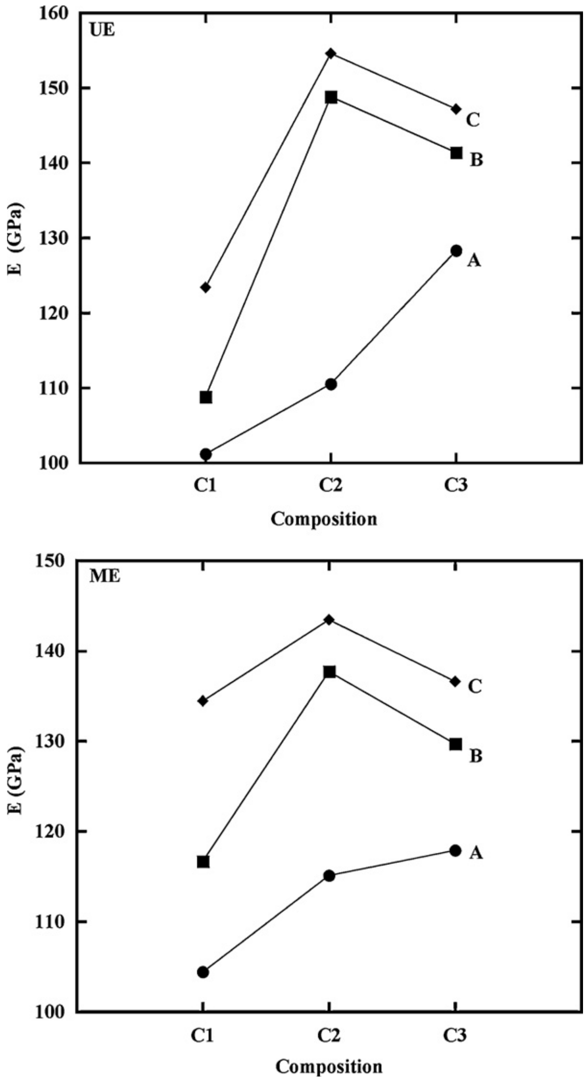

Fig. 9. Variation of the Young's modulus of samples sintered at A = 1450 °C (●), B = 1550 °C (■) or C = 1650 °C (◆). UE = Young's modulus determined by ultrasound technique and ME = Young's modulus obtained by mechanic testing.

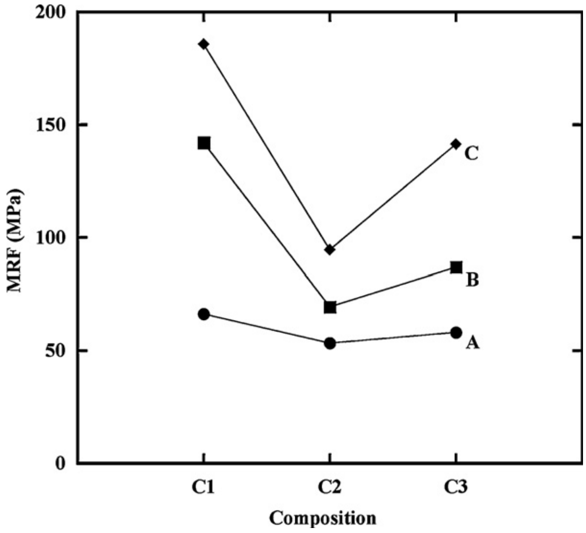

Fig. 10. Variation of maximum resistance to fracture (MRF) for samples sintered at A = 1450 °C (●), B = 1550 °C (■) or C = 1650 °C (◆).

the difference observed between the values of the MOF determined in this work and that are reported in the literature [20] for similar refractory materials, which could be related to the use of two different raw materials (zirconia vs. zircon) for their synthesis.

3.6. Fracture analysis

A fractographic study was conducted with the primary purpose of knowing the mechanism of propagation of cracks in the tested specimens using the scanning electron microscopy. Fig. 11 shows the micrographs of compositions C1, C2 and C3 sintered at 1650 °C. In general, the fractographic analysis revealed that this compositions presented intergranular fracture. At first sight, the fracture surface showed a granular texture, which could have resulted from orientation changes that took place in the cleavage planes within the grains or along the grain boundaries, causing crack propagation through the matrix material. This type of fracture usually occurs after a process that weakens or fragilizes the region of the grain boundaries [21–23].

3.7. Vickers microhardness

The highest Vickers microhardness obtained for the studied compositions was 235 kgf/mm^2. In general, the samples of all studied compositions had a relatively low Vickers microhardness, probably because as temperature increased, they suffered a significant increase in the size of the zirconia particles, as well as in the amount of porosity; both factors reduce the hardness of the materials. It has been reported that the average size of the ZrO_2 particles has a significant impact on the hardness values [3,24]. Fig. 12 shows graphically the variation of microhardness for each one of the studied compositions at different sintering temperatures.

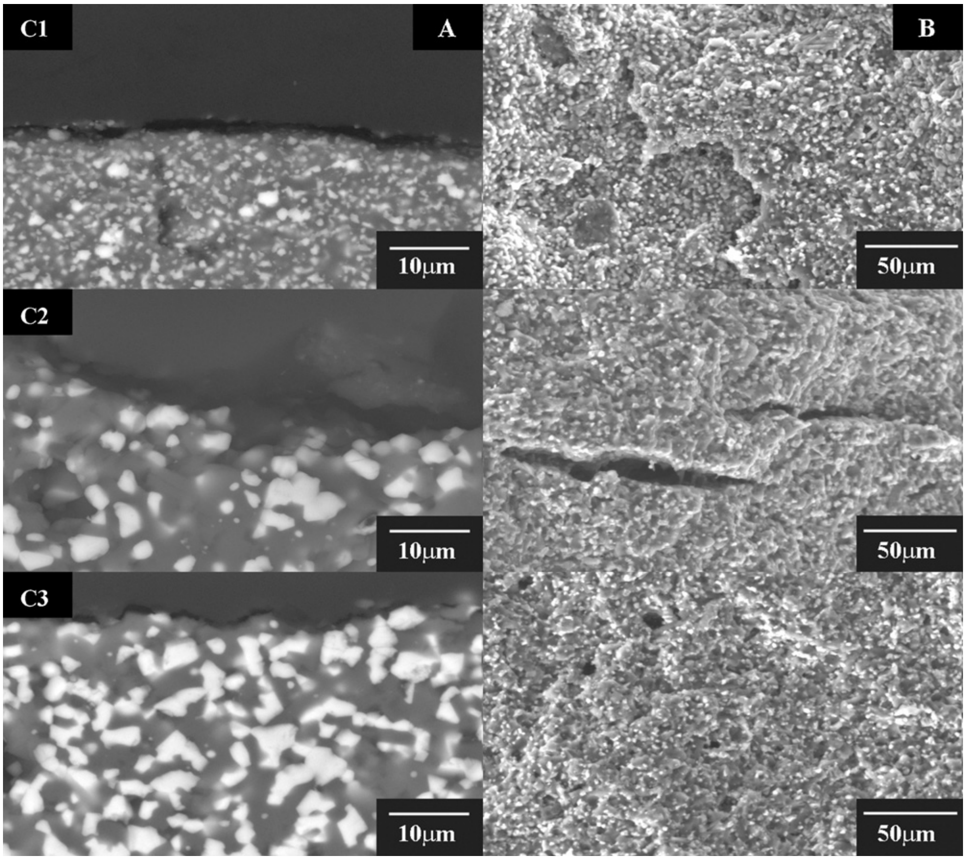

Fig. 11. Fracture surface of compositions C1, C2 and C3 sintered at 1650 °C (A) cross sectional micrographs, and (B) fracture surface micrographs.

3.8. Fracture toughness (critical stress intensity factor K_{IC})

Fig. 13 shows graphically the values obtained for each one of the studied compositions sintered at different temperatures. The highest K_{IC} value was obtained at 1650 °C. This was attributed to the zirconia crystal growth [3]. This means that the effect of the zirconia grain size on the value of K_{IC} was contrary to that caused by the same factor on the values of Young's modulus and Vickers microhardness.

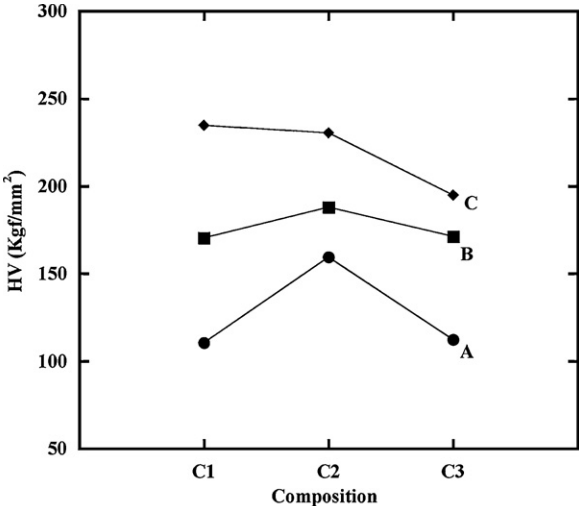

Fig. 12. Variation of Vickers microhardness (HV) for samples sintered at A = 1450 °C (●), B = 1550 °C (■) or C = 1650 °C (◆).

3.9. General discussion of mechanical properties

It is important to mention that the results of all mechanical properties are influenced by the composition and the matrix in the micrographs showed before, due to the porosity, the particle size of the phases, the presence of one or other phases in the microstructures and the sintering temperature. In general it was

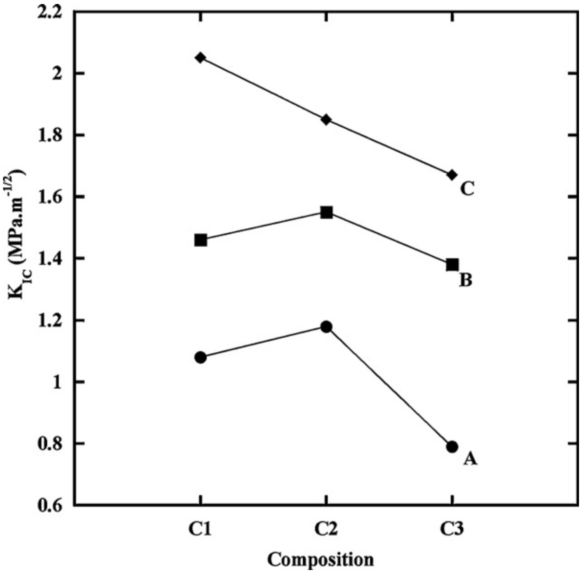

Fig. 13. Variation of fracture toughness (K_{IC}) for samples sintered at A = 1450 °C (●), B = 1550 °C (■) or C = 1650 °C (◆).

observed that at higher temperatures (1650 °C) the compositions had a better mechanical performance compared to those sintered at 1550 °C, due to the densification achieved at the former temperature, as well as to the formation of cracks in the samples after sintering caused by the polymorphic transformations of zirconia and the volumetric expansion of this material [7–9,25], and also because of the percentages of kaolin added to the compositions since kaolin volumetric changes increased formation of cracks in the samples [18].

4. Conclusions

The compositions sintered at 1650 °C had a better mechanical performance compared to those sintered at 1550 °C, due to the formation of cracks at the latter temperature caused by the polymorphic transformations of zirconia. For all studied compositions, the X-ray diffraction and SEM characterization confirmed in general the formation of the phases predicted according to the ternary phase diagram Al_2O_3–ZrO_2–SiO_2, in varying amounts of each phase formed. The crystalline phases identified in the sintered materials were: Al_2O_3, monoclinic ZrO_2, tetragonal ZrO_2, $Al_6Si_2O_{13}$ and $ZrSiO_4$. The formation of the latter phase at 1450 °C in compositions C1 and C2, which was not expected according to the ternary phase diagram, was attributed to the reaction occurring between the added ZrO_2 and SiO_2 contained in kaolin. For composition C1, SEM characterization showed significant microstructural differences between samples sintered at 1550 and those sintered at 1650 °C, particularly regarding the size of the ZrO_2 particles. The results of the evaluation of mechanical properties showed that the values of Young's modulus obtained by ultrasonic and mechanical tests were very similar, mainly because the latter tests take into account the distribution of defects in the samples. Lastly, the growth of zirconia particles as temperature increased had a significant effect on the measured mechanical properties, causing a decrease in the Vickers microhardness of the samples while fracture toughness (K_{IC}) was increased by it.

Acknowledgement

To the National Council of Science and Technology (CONACYT) for the resources provided for the development of this work.

References

[1] E.V. Bychkov, Baddeleyite–Corundum refractories for the glass industry, Refractories and Industrial Ceramics 40 (1999) 69–71.

[2] L.L. Chernina, N.A. Yavtukhovich, A.N. Oleinikova, V.E. Ignatov, Some features of the service of bakor refractories, Glass and Ceramics 26 (2) (1969) 14–16.

[3] D. Sarkar, S. Adak, M.C. Chu, S.J. Cho, N.K. Mitra, Influence of ZrO_2 on the thermo-mechanical response of nano-ZTA, Ceramics International 33 (2007) 255–261.

[4] A.G.M. Othman, W.M.N. Nour, Recycling of spent magnesite and AZS bricks for the production of new basic refractories, Ceramics International 31 (8) (2005) 1053–1059.

[5] A. Rafferty, A.M. Alsebaie, A.G. Olabi, T. Prescott, Properties of zirconia-toughened–alumina prepared via powder processing and colloidal processing routes, Journal of Colloid and Interface Science 329 (2009) 310–315.

[6] G.W. Nieman, J.R. Weertman, R.W. Siegel, Journal of Materials Research 6 (1991) 1012–1027.

[7] T. Asokan, Exudation behaviour of heat treated Al_2O_3–ZrO_2–SiO_2 fusion cast refractories, Journal of Materials Science Letters 14 (18) (1995) 323–1326.

[8] T. Asokan, Microstructural features of fusion cast Al_2O_3–ZrO_2–SiO_2 refractories, Journal of Materials Science Letters 13 (5) (1994) 343–345.

[9] M.H. Bocanegra Bernal, S. Diaz de la Torre, Phase transitions in zirconium dioxide and related materials for high performance engineering ceramics, Journal of Materials Science 37 (2002) 4947–5497.

[10] H.M. Ondik, H.F. McMurdie, Phase Diagrams for Zirconium + Zirconia Systems, 1st edition, The American Ceramic Society, USA, 1998.

[11] G.I. Vázquez Carbajal. Estudio de la obtención de Materiales Refractarios tipo ZAS. Tesis de Maestría. CINVESTAV-IPN, Unidad Saltillo, 2007.

[12] Norma ASTM E 494-95. Standard Practice for Ultrasonic Velocity in Materials.

[13] Norma ASTM E 797-95. Standard Practice for Measuring Thicness by Manual Ultrasonic Pulse-Echo Contact Method.

[14] Norma ASTM C 1161-94. Standard Test Method for Flexural Strength of Advanced Ceramics at Room Temperature.

[15] Norma ASTM E 92-82. Standard Test Method for Vickers Hardness of Metallic Materials.

[16] R. McPherson, R. Rao, B.V. Shafer, The reassociation of plasma dissociated zircon, Journal of Materials Science 20 (1985) 2597–2602.

[17] M.N. Arman, Ceramic Processing and Sintering, 1st edition, Marcel Dekker Inc., New York, USA, 1995.

[18] N.V. Pitak, R.M. Fedoruk, T.P. Khmelenko, R.S. Shulyak, V.Kh. Zima, I.P. Davydov, R.E. Shcherbina, G.A. Belokrys, High-density kaolin refractories, Institute of Refractories 1 (1978) 8–14.

[19] W. David, Richerson, Modern Ceramic Engineering, Properties, Processing and Use in Design, 2nd edition, Marcel Dekker Inc., New York, USA, 1992.

[20] A.C. Mazzei, J.A. Rodrigues, Alumina–mullite–zirconia composites obtained by reaction sintering, Journal of Materials Science 35 (2000) 2807–2814.

[21] R. Echeverria. Fractura de Materiales. Universidad Nacional del Comahue, 2003.

[22] W.D. Kingery, H.K. Bowen, D.R. Uhlmann, Introduction to Ceramics, 2nd edition, John Wiley and Sons, A Wiley-Interscience Publication, New York, USA, 1976.

[23] M.V. Ramos Ramírez Estudio del comportamiento mecánico de materiales de MgO–$CaZrO_3$–Ca_2SiO_4 or $Ca_3Mg(SiO_4)_2$ Tesis de maestría en ingeniería cerámica. CINVESTAV-IPN Unidad Saltillo, 2006.

[24] LIANG. Shu-quan, T.A.N. Xiao-ping, L.I. Shao-qiang, T.A.N.G. Yan, Structure and mechanical properties of ZrO_2–mullite nano-ceramics in SiO_2–Al_2O_3–ZrO_2 system, Journal of Central South University of Technology 14 (2007) 1–6.

[25] J.F. Shackelfors, R.H. Doremus, Ceramic and Glass Materials: Structure Properties and Processing, Springer, 2008 Chapter 1, Chapter 10.